Supplementary Information：Realization of electron antidoping by modulating the breathing distortion in $BaBiO_3$

Hui Cao[1,2‡], Hongli Guo[1,3‡], Yu-Cheng Shao[4], Qixin Liu[1], Xuefei Feng[4], Qinwen Lu[1], Zhengping Wang[1], Aidi Zhao[1,5], Atsushi Fujimori[6], Yi-De Chuang[4], Hua Zhou[2*], and Xiaofang Zhai [1,5*]

[1] *Department of Chemical Physics, Department of Physics, Physics Experiment Teaching Center, and Hefei National Laboratory for Physical Sciences at the Microscale, University of Science and Technology of China, Hefei 230026, China*

[2] *X-ray Science Division, Advanced Photon Source, Argonne National Laboratory, Lemont, IL 60439, USA*

[3] *School of Physics and Technology and Key Laboratory of Artificial Micro- and Nano-Structures of Ministry of Education, Wuhan University, Wuhan 430072, China*

[4] *Advanced Light Source, Lawrence Berkeley National Laboratory, Berkeley, CA 94720 USA*

[5] *School of Physical Science and Technology, ShanghaiTech University, Shanghai 201210, China*

[6] *Department of Applied Physics, Waseda University, Okubo, Shinjuku, Tokyo 169-8555, Japan*

Section I. XRD characterization of lattice constants

The reciprocal space map (RSM) measurements were done to detect the in-plane lattice constants of the $BaBiO_3$ and $BaBiO_{3-\delta}$ films, with the results shown in Supplementary Fig. 7. We measured the lattice structure of the $BaBiO_3$ and $BaBiO_{3-\delta}$ films using high-resolution x-ray diffraction (XRD). The monochromatic X-rays were provided by Cu $K_{\alpha 1}$ (λ = 0.154056 nm and $\Delta\lambda/\lambda$ ~23 ppm), the beam divergence was 12 arc sec. An additional monochromator with a two-bounce Ge (220) channel-cut analyzer was placed in front of a proportional counter in the diffracted beam path with the same beam divergence. For polar angle (θ) and tilt angle (φ), the angular precision and reproducibility of the diffractometer are 0.0001° and 0.0003°, respectively. The (0 0 *L*) specular reflection of the $BaBiO_3$ and $BaBiO_{3-\delta}$ films around *L*=2 exhibits clear thickness oscillation fringes (see Supplementary Fig. 8a), demonstrating the high quality of these thin film samples. Both in-plane and out-of-plane lattice constants of these films are plotted in Supplementary Fig. 8b. As the amount of O_vs increases, the out-of-plane lattice constant *c* increases from 4.34(0) Å to 4.35(8) Å while the in-plane lattice constant *a* decreases from ~4.38 Å to 4.35(3) Å. Overall, the lattice transforms from a slightly tetragonal ($a > c$) structure to a pseudocubic ($a \approx c$) structure. Such a structural transition and the almost conserved unit cell volume agree with the bulk study of $BaBiO_{3-\delta}$ in the range of $0 \leq \delta \leq 0.25$ (1).

Section II. Details of X-ray absorption and emission spectroscopy measurements

For the O K-edge XAS and XES measurements, all thin-film samples were attached to

the sample holders with carbon tapes and transferred from airside into the high vacuum experimental chamber (pressure better than 8×10^{-9} torr) through a load-lock system. All measurements were carried out at room temperature with the beamline energy resolution set to ~ 0.4 eV at O K-edge and π-polarization in the horizontal scattering plane. The sample surface was at 30° grazing incidence angle and a GaAsP photodiode located at 150° emission angle relative to the incident x-ray beam was used to record the XAS spectra. This photodiode, with an angular acceptance of 30 mrad (both vertical and horizontal), has a frontal Al window to block out the ambient visible light and photoelectrons. For XES, the excitation photon energy was set to 570 eV, far above the O absorption edge. A modular X-ray spectrometer at 140° emission angle was used to record the XES spectra (2). The combined energy resolution (~ 0.4 eV, beamline plus spectrometer) and the calibration for XES spectra (converting the detector pixel number to emission energy) were determined using the elastic line from a carbon tape next to the samples. This method ensures the proper energy alignment between XAS and XES to be better than 0.05 eV.

Section III. Details of Raman spectroscopy, XRD half-order Bragg peak measurement and quantification of oxygen octahedral rotations

Raman spectra were measured using a laser confocal spectrometer with an excitation wavelength of 514 nm and a magnification level of 100. The spectra were obtained with a laser spot size of about 1 μm, an illumination power less than 20 mW, and an

integration time of 10 sec. The spectral resolution for the incoming 514 nm light is 0.65 cm^{-1}.

It is known that the oxygen-octahedral-rotation (OOR) induces a unique XRD intensity profile of half-order Bragg peaks, which can be utilized to determine the rotation angles (3-5). For detailed XRD half-order-peak investigations, the XRD measurements used hard X-Rays source of sector 33BM of the Advanced photon Source at room temperature. To rule out the fluorescence signal of the substrate, the high energy (E = 16 keV) of X-Ray has been chosen. The geometric corrections and background subtractions were done for all data. Then we analyzed the data using the previous fitting procedure (3-6). In $BaBiO_3$, in addition to the OOR, the breathing distortion also doubles the unit cells along each of the pseudocubic axis, resulting in a supercell with 24 oxygen atoms which is similar to the OOR effect. In Supplementary Fig. 11, the BiO_6 octahedra are shown to collapse and expand alternately along with the three pseudocubic crystallographic directions. Here the positions of the oxygen atoms are first individually calculated from the rotation matrix as in previous literature (3-5). Then the oxygen position is further modulated by the bond length correction due to the breathing distortion. The rotation angles α, β and γ are along the pseudocubic *a*, *b* and *c* axis, respectively. The breathing distortion Δ defines the bond variation, with the collapsed bond and elongated bond length to be $(1-\Delta)L$ and $(1+\Delta)L$ respectively. L is the average bond length of Bi-O but is not appearing in the half order peak profile calculation (3-5). For example, in Fig. S11, the Bi-O bond lengths in the #1, #4, #6 and #7 octahedra are $(1+\Delta)L$, and the Bi-O bond lengths in the #2, #3, #5 and #8 octahedra

are (1-Δ)L. By considering both the rotations and the bond length variations, the positions of 24 oxygen atoms are all defined by the four independent variables of α, β, γ and Δ. The typical fitting results of $BaBiO_{2.92}$ are shown in Supplementary Fig. 12.

Supplementary Table 1: The positions of atoms in primitive cell of monoclinic $BaBiO_3$ unit cell.

Atom label	Position (x, y, z)
Ba1	(0.249629, 0.750371, 0.741814)
Ba2	(0.750371, 0.249629, 0.258186)
Bi1	(0.000000, 0.000000, 0.000000)
Bi2	(0.500000, 0.500000, 0.500000)
O1	(0.702278, 0.785292, 0.699562)
O2	(0.785292, 0.702278, 0.300438)
O3	(0.297722, 0.214708, 0.300438)
O4	(0.214708, 0.297722, 0.699562)
O5	(0.258392, 0.741608, 0.183981)
O6	(0.741608, 0.258392, 0.816019)

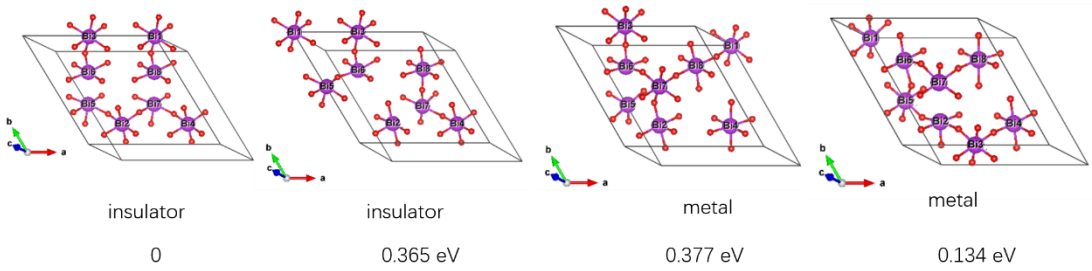

Supplementary Figure 1 Four different configurations with different O_v locations in $BaBiO_{2.75}$; the most stable one is identical to that in the main text.

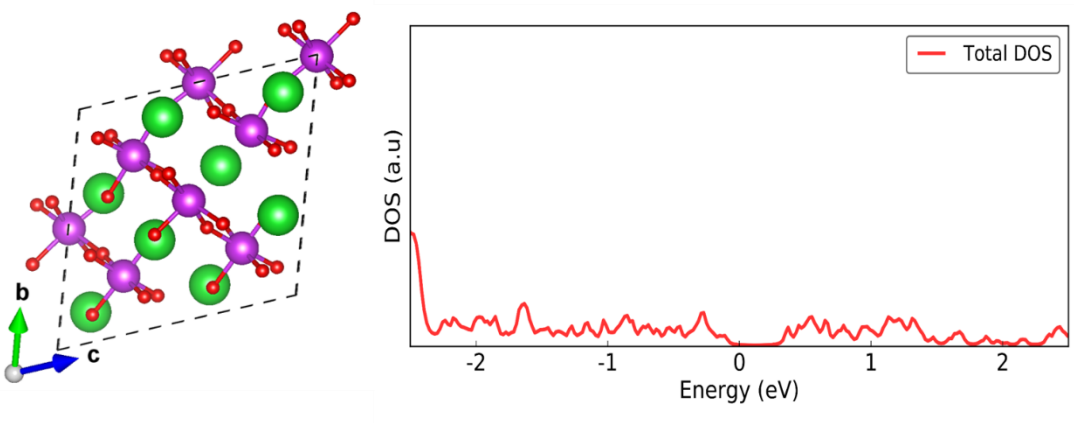

Supplementary Figure 2 Left: configuration of a 2x2x2 supercell with 2 O_vs ($BaBiO_{2.875}$); Right: the DOS of $BaBiO_{2.875}$, still showing an insulating gap.

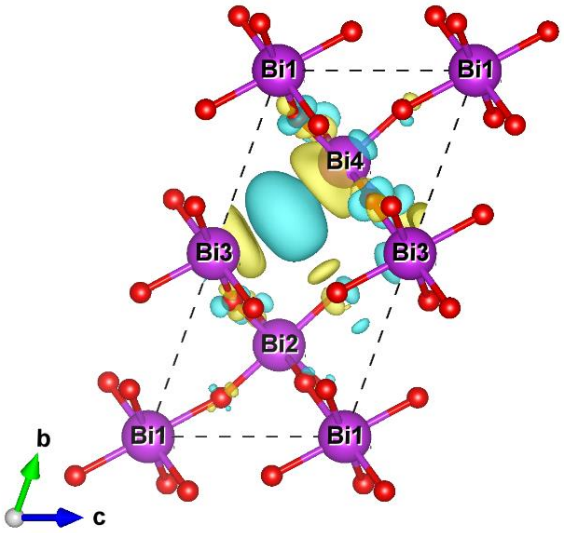

Supplementary Figure 3 The difference charge density map of $BaBiO_{2.75}$, the yellow iso-surface represents the charge accumulation, and blue iso-surface represents the charge depletion. From the difference charge density, we can see that the electrons are transferred from the oxygen vacancy site to both Bi3 and Bi4 atoms; however, Bi4 atom gets more electrons than Bi3. In addition, charge transfer also happens at the oxygen sites.

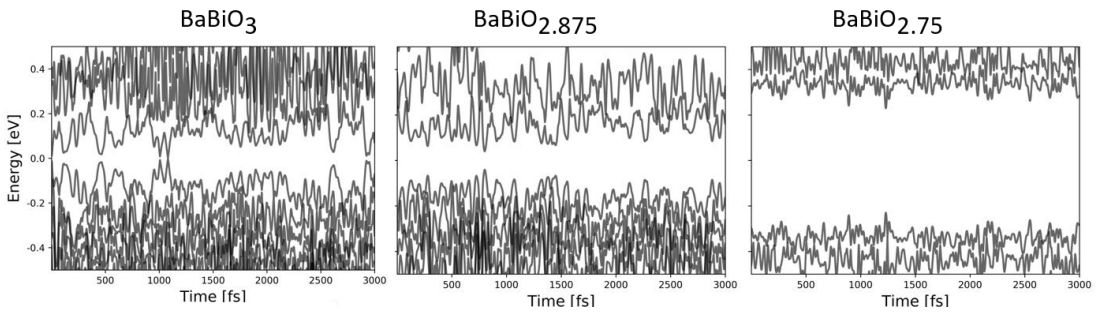

Supplementary Figure 4 Time evolutions of energy states of $BaBiO_3$, $BaBiO_{2.875}$, $BaBiO_{2.75}$ in MD simulation at 300 K, showing band gap enhancement with electron doping.

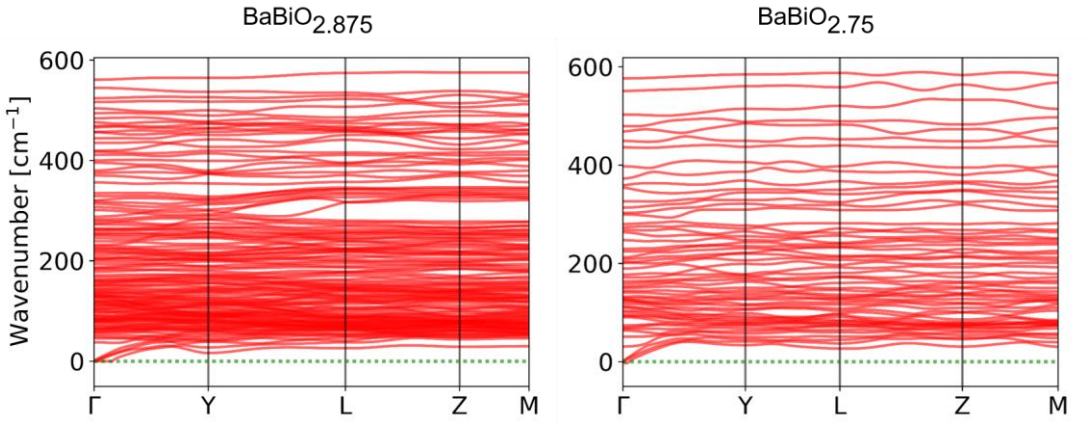

Supplementary Figure 5 The phonon band structures of $BaBiO_{2.875}$ and $BaBiO_{2.75}$, no negative phonon frequency is found, indicating the structural stability when the oxygen vacancy is introduced.

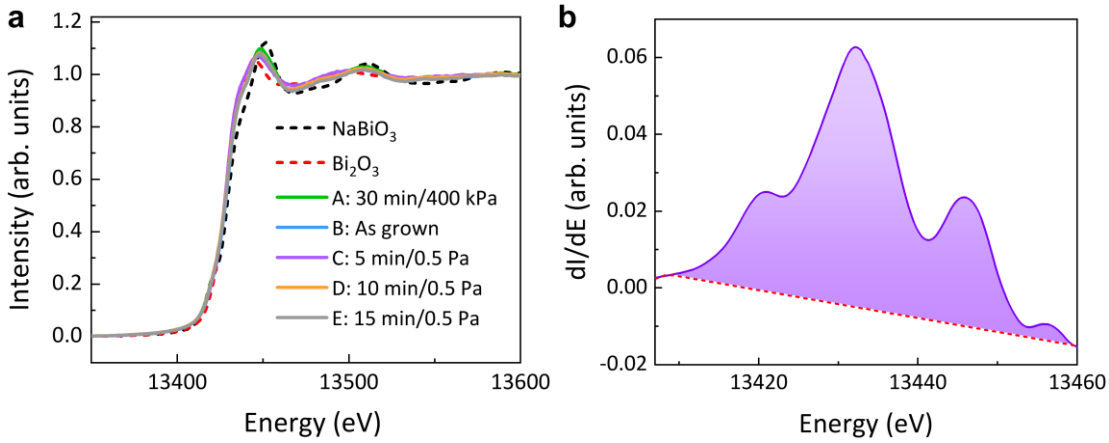

Supplementary Figure 6 (a) Bi L_3-edge XANES spectra of the $BaBiO_{3-\delta}$ ($0 \leq \delta \leq 0.25$) thin films and two reference samples. (b) Integration graph of dI/dE.

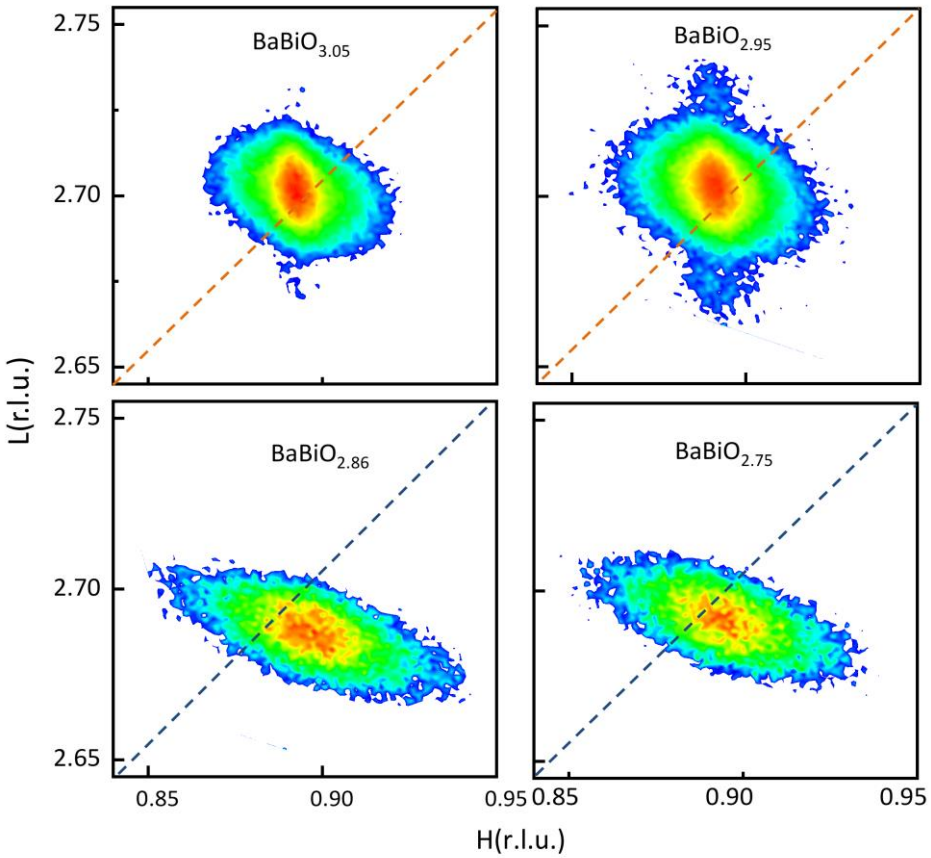

Supplementary Figure 7 XRD reciprocal space maps of $BaBiO_{3-\delta}$ thin films taken around the (1 0 3) film diffraction peaks; the reciprocal lattice units (r.l.u.) are drawn using the $SrTiO_3$ substrate lattice constants and all thin films are relaxed. The intensity is shown on a logarithmic scale. The dashed lines are guides for eye.

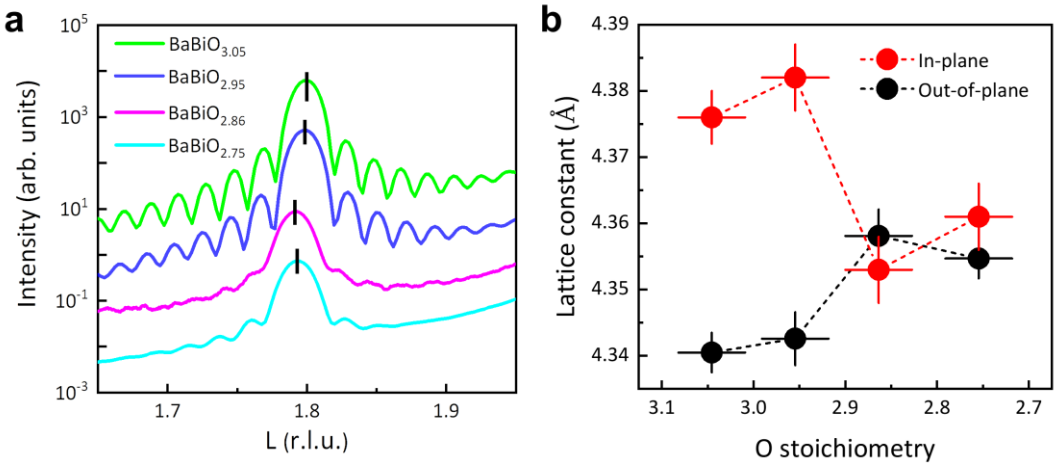

Supplementary Figure 8 (a) Specular 00L XRD data (H, K=0) for the thin films near L=2, in reciprocal lattice units (r.l.u.) of $SrTiO_3$; the spectra are vertically shifted for clarity. The peaks of thin films are indicated by black lines. The thickness Laue fringes are very pronounced. (b) In-plane and out-of-plane lattice constants of the four sets samples. The dashed lines are guides for eye.

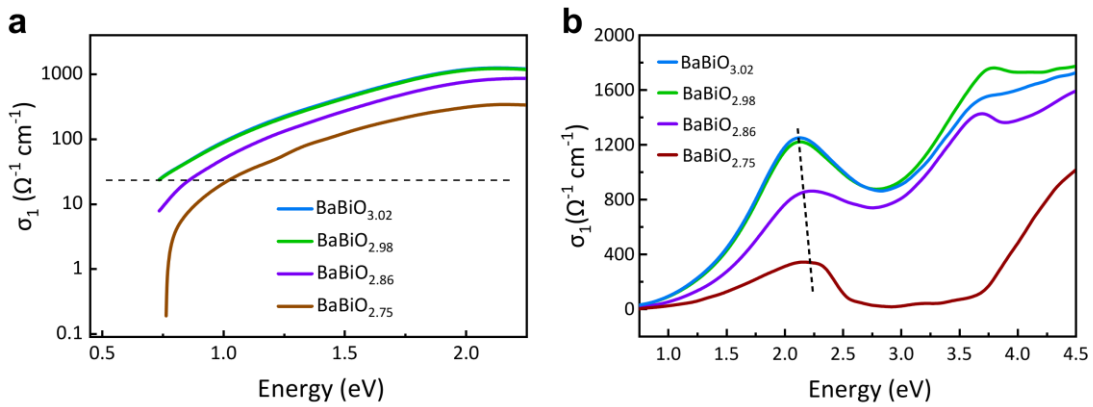

Supplementary Figure 9 (a) The method to find the photon energy at which the optical conductivity has a very small value of 23 Ω^{-1} cm^{-1}, indicated by the dashed line, in the $BaBiO_{3-\delta}$ ($0 \leq \delta \leq 0.25$) thin films. (b) The large range real part of optical conductivity σ_1 measured via spectroscopic ellipsometry.

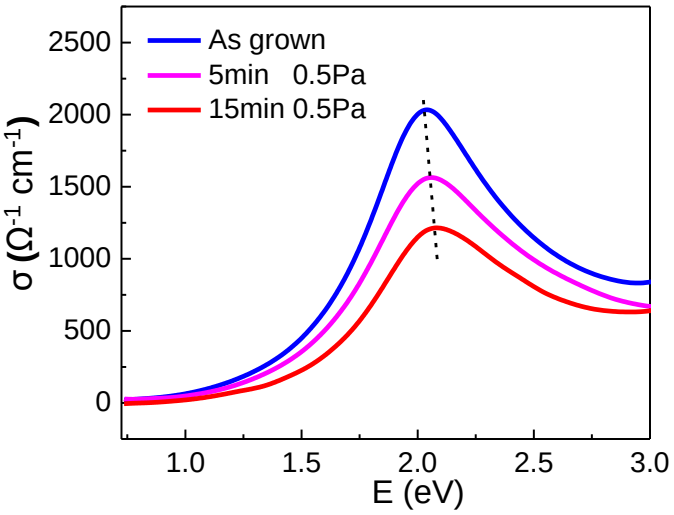

Supplementary Figure 10 The optical conductivity of another group of samples without any oxygen stoichiometry quantification.

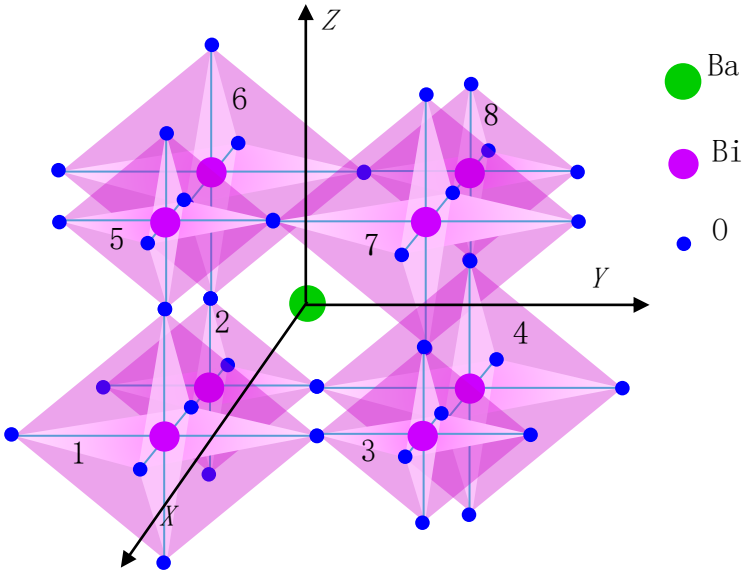

Supplementary Figure 11 Definition of a coordinate system within a super unit cell of 2x2x2 as a result of breathing distortion.

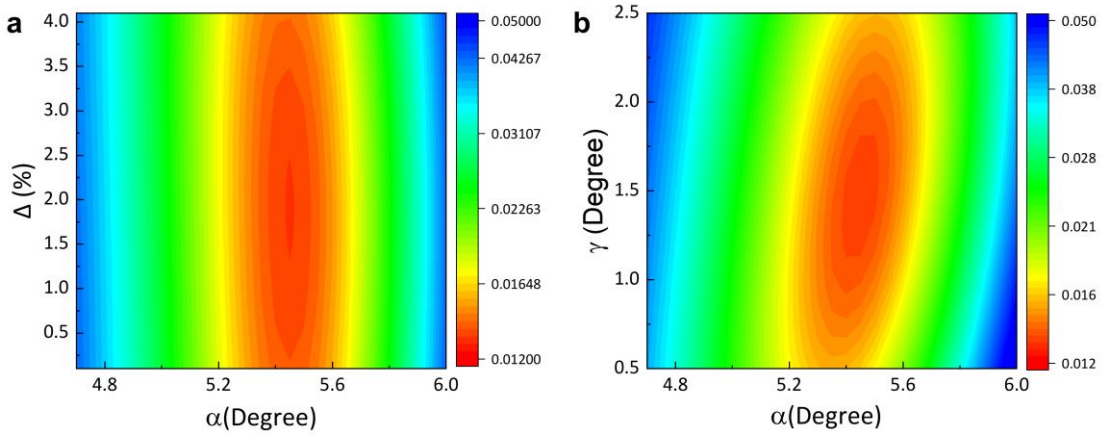

Supplementary Figure 12 Figure of merit of fitting goodness for oxygen octahedral rotation angles and lattice breathing distortions of $BaBiO_{2.92}$ (a) with β and γ fixed at the optimal values and (b) with β and Δ fixed at the optimal values.

Supplementary References:

[1] Kambe, S. et al. Crystal structure and electronic properties of $BaBiO_y$ ($2.5 \leq y \leq 2.9$) and $Ba_{1-x}La_xBiO_3$ ($0 \leq x \leq 0.5$). *Solid State Ion.* **108,** 307 (1998).

[2] Chuang, Y.-D. et al. Modular soft x-ray spectrometer for applications in energy sciences and quantum materials. *Rev. Sci. Instrum.* **88,** 013110 (2017).

[3] May, S. J. et al. Quantifying octahedral rotations in strained perovskite oxide films. *Phys. Rev. B* **82,** 01110 (2010).

[4] May, S. J. et al. Control of octahedral rotations in $(LaNiO_3)_n/(SrMnO_3)_m$ superlattices. *Phys. Rev. B* **83,** 153411 (2011).

[5] Hovestreydt, E. On the atomic scattering factor for O^{2-}. *Acta Cryst. A* **39,** 268-269 (1983).

[6] Zhai, X. et al. Correlating interfacial octahedral rotations with magnetism in $(LaMnO_{3+\delta})_N/(SrTiO_3)_N$ superlattices. *Nat. Commun.* **5,** 4283 (2014).